DOI: 10.1002/ejic.200800538

Processing and Characterization of Spherical Alumina Pellets Coated with $BaTiO_3$ and $Li_{0.10}Ti_{0.02}Ni_{0.88}O$ Dielectric Materials

Benoit Fournaud,[a] Alexandra Iordan,[b] Sylvie Rossignol,*[c] Jean-Michel Tatibouët,[a] and Stephanie Thollon[d]

Keywords: Dielectric materials / Sol–gel processes / Coating / Spherical pellets / Electron microscopy

Sol–gel methods were used to synthesize $BaTiO_3$ and $Li_xTi_yNi_{(1-x)}$ materials. Processes using these sols were adjusted to coat spherical alumina pellets. The annealing temperature was studied in detail. This study also focuses on the characterization of the deposits. Data obtained by XRD, scanning electron microscopy, Raman spectroscopy, and gravimetric analyses were compared. Multiple impregnations were necessary to achieve a satisfactory deposit of the dielectric material. For $Li_{0.10}Ti_{0.02}Ni_{0.88}O$, these sol–gel methods led to an impregnation depth of 50 μm, whereas for $BaTiO_3$ a homogeneous deposit of only 5 μm was obtained. A special treatment with an ammonia solution was required to efficiently disperse $BaTiO_3$. This preparation method achieved a spherical deposit of the dielectric material.

Introduction

In the last few years, nonthermal plasma technology has become of increasing interest in the catalysis field. This technology was employed effectively to treat exhaust gas flow.[1] Nonthermal plasma has many advantages compared to the classical catalysis technology: among other things, the system is efficient and, most of all, it requires less energy. Moreover, research has shown that dielectric materials (i.e. with a high dielectric constant) in the plasma zone need lower power.[2] Materials with high dielectric constants are used in the microelectronic industry for the manufacturing of condensers.[3] Many studies were carried out on different classes of materials. PZT (lead zirconate titanate) materials were often studied,[4,5] but the occurrence of Pb limited the scope of such materials. Perovskite materials and barium titanate appeared to be interesting alternatives.[6,7] Some of these studies focused on the insertion or substitution of doping elements to increase the dielectric properties,[8,9] whereas others focused on doping elements to decrease the calcination temperature.[10] The actual synthesis was also studied.[11,12] Among these methods, the synthesis of a pure cubic phase was achieved from a mixture of alkoxides with barium carbonate at a final treatment temperature of 800 °C.[13] Despite the high cost of the precursors, the sol–gel process is attractive for the preparation of advanced ceramics because they can be obtained in high purity and homogeneity.[14] Another recently discovered family of materials are nickel oxides with lithium and titanium dopants.[15,16] To be used in a nonthermal plasma reactors, dielectric materials must be shape formed. Massive shape-forming could be performed by extrusion[17] or oil-drop processes.[18] The use of dielectric materials in microelectronics have led to developments in 2D thin film processes. Powders of dielectric materials can be deposited by using an electric field[19] or by radio frequency (rf)magnetron sputtering.[20] A deposit can also form from a sol by metal-organic chemical vapour deposition,[21] spin coating[22] or ink-jet printing.[23] However, at this time, no research has been done on the depositing of dielectric materials on a spherical surface. The novelty of this work lies in the preparation of dielectric deposits on spherical alumina balls with a nonthermal plasma application method.

Chemical processes are only feasible if there are interactions between substrate and material. To characterize these interactions, various analyzing methods like X-ray diffraction or scanning electron microscopy (SEM) can be used. With Raman spectroscopy, a part of the sample can be efficiently focused on by equipping the spectrometer with microscope optics. The radius of curvature no longer influences the results. This technique cannot be used for $Li_xTi_yNi_{1-x-y}O$ materials because of their fluorescence, but it may be adapted for $BaTiO_3$ materials. Peaks resulting from the tetragonal or cubic phases of $BaTiO_3$ are well known and have been identified.[24,25] However, some conflicting results are noted in the literature, for example, a cubic phase identified by XRD appears in Raman spectroscopic analyses like a tetragonal phase.[26,27] This inconsistency is due

[a] LACCO, UMR6503,
40 Av Recteur Pineau, 86002 Poitiers Cedex, France
[b] I. Cuza University,
Bulevardul Carol I Nr. 11, Iasi 6600, Romania
[c] GEMH, ENSCI,
47 à 73 Av Albert Thomas, 87065 Limoges Cedex, France
Fax: +33-5-55-45-22-22
E-mail: Sylvie.rossignol@unilim.fr
[d] CEA Grenoble, DRT/DTNM/LITEN/LTS,
17, rue des Martyrs, 38054 Grenoble Cedex 9, France

to the particle size of the material.[28,29] In fact, a particle size between 30 nm and 100 nm led to a pseudocubic phase,[30] which can be described as a global cubic structure with local tetragonal clusters.[31] Raman spectroscopy cannot be used to identify the phases of $BaTiO_3$, but it can be used to determine the coating properties of $BaTiO_3$.

The aim of this work was to synthesize a coating for $BaTiO_3$ and $Li_xTi_yNi_{1-x-y}O$ compounds on the surface of spherical alumina pellets. The interaction between the support and the dielectric materials must be limited in order to preserve the efficient dielectric properties. In the first part, the syntheses of powders allowed us to adjust the sol preparation for each material. In the second part, optimal sols were used in a specific treatment to coat spherical pellets. The morphology of the deposit was observed by scanning electronic microscopy (SEM). The deposit was characterized by gravimetric analyses, surface area and X-ray diffraction methods, and the results were compared with that of the original powders.

Results and Discussion

Powder Samples

LiTiNiO

The thermogravimetric (TG) analyses of dry powders show a precursor decomposition below 500 °C regardless of the protocol (Figure 1a). This decomposition was very fast in the case of the P_b protocol (see Experimental Section for more details) and took place in one step near 400 °C (Figure 1b). For the P_a protocol, two steps are shown in the differential thermal (DT) analysis, particularly in the case of the second doping agent ($Li_{0.222}Ti_{0.045}Ni_{0.733}O$-$P_a$). These two steps correspond to the decomposition of the nickel and lithium precursors[32,33] and to that of the titanium precursor.[34] The increase in doping agents tended to shift the decomposition temperature, thereby displaying that a critical energy was required to decompose the precursor of such nitrate-containing doping agents. On the contrary, the fast and unique decomposition of the powder prepared by the P_b protocol revealed that $Li_{0.10}Ti_{0.02}Ni_{0.88}O$ was directly formed at a temperature of 500 °C.

After thermal treatment at 500 °C, the X-ray powder patterns for both procedures are characteristic of a NiO single cubic phase (Figure 2); no other peaks due to doping elements could be detected. Consequently, the introduction of lithium and titanium elements involved the formation of a solid NiO solution, as mentioned by Maensiri et al.[35] Indeed, Ni^{2+} (0.69 Å) ions can easily be replaced by Li^+ (0.68 Å) or Ti^{4+} (0.68 Å) ions in the lattice structure of NiO because of their similar radii.

The particle sizes determined by Debye–Scherer methods (D_{XRD}) were similar for all three samples (Table 1), even if the surface area values are dependent on the protocol used. Furthermore, considering that the particles were spherical, their size could be determined from BET measurements according to Equation (1):

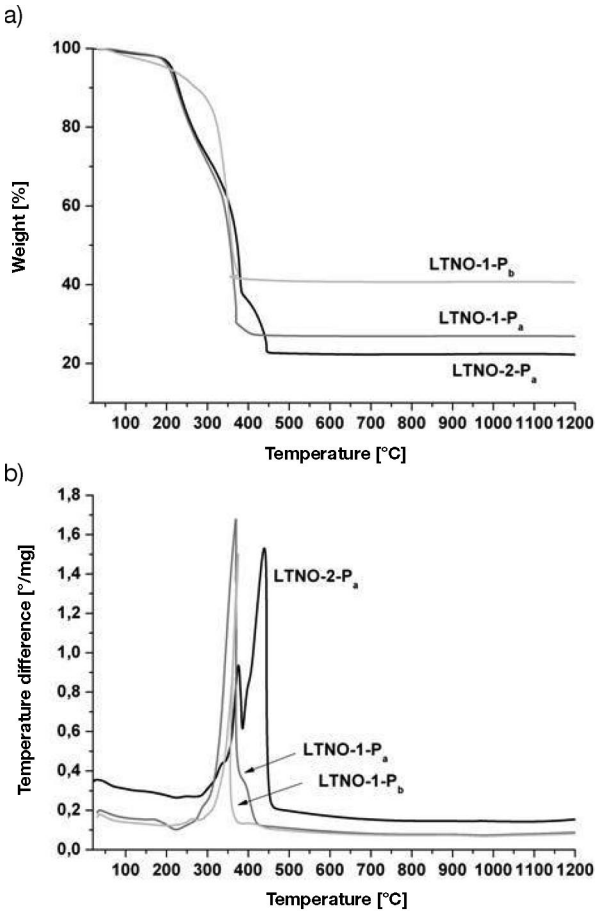

Figure 1. a) Thermogravimetric and b) differential thermal curves of $Li_{0.10}Ti_{0.02}Ni_{0.88}O$ (LTNO-1) and $Li_{0.222}Ti_{0.045}Ni_{0.733}O$ (LTNO-2) powders.

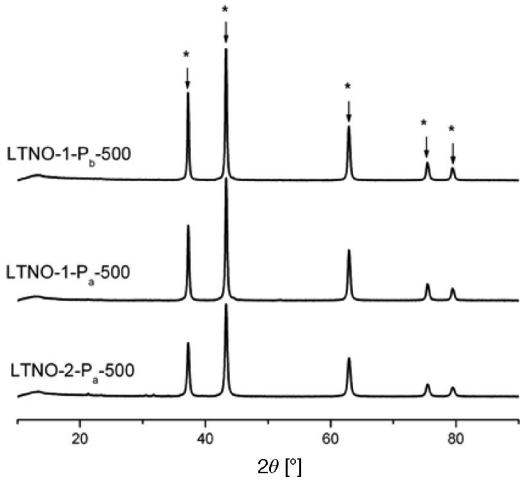

Figure 2. XRD patterns for the different protocols for LTNO with annealing at 500 °C (PDF file:* NiO 78–0429).

$$S_{BET} = \frac{4\cdot\pi\cdot(D_{BET}/2)^2}{4/3\cdot\pi\cdot(D_{BET}/2)^3\cdot\rho_{material}} \quad (1)$$

Table 1. Surface area and particle size determined from BET or XRD for the powders synthesized as a function of annealing temperature.

Sample	Annealing temperature[°C]	S_{BET} [$m^2 g^{-1}$]	D_{BET} [nm]	D_{XRD} [nm]
LTNO-1-P_a	500	15	29	18
LTNO-2-P_a	500	15	29	22
LTNO-1-P_b	500	4	110	23
BT-P_1-500	500	–	–	–
BT-P_2-500	500	–	–	–
BT-P_1-800	800	–	–	–
BT-P_2-800	800	10	45	25

Because of the low doping, the theoretical density of NiO was used. The particle sizes calculated for the P_a procedure were smaller than those calculated for the P_b procedure. The particle sizes determined from these data imply that an important aggregate in the P_b procedure ($D_{BET} > D_{XRD}$) has emerged. For this reason, the P_a procedure was used to deposit $Li_xTi_yNi_{(1-x)}$ on alumina balls. It can be noted that the proportions of the doping agent did not affect the structural properties of the powders. We chose to deposit $Li_{0.10}Ti_{0.02}Ni_{0.88}O$ over the alumina balls.

$BaTiO_3$

Thermogravimetric and differential thermal analyses (Figure 3) reveal that decomposition of the precursors occurred in three steps for the P_1 and P_2 procedures (see Experimental Section for more details, Table 3). For both procedures, the first step between 25 °C and 250 °C has been attributed to the vaporization of water and small organic compounds. For the P_1 and P_2 procedures, the peaks in the DT curves between 200 °C and 500 °C are due to the decomposition of acetate groups and the simultaneous formation of complexes containing Ti.[37] The last peak can be associated to the formation of the perovskite phase.

To understand more precisely which phenomena takes place, both powders were annealed first at 500 °C (where a step can be found on the thermograms of the two samples) and then at 800 °C. The X-ray powder diffraction pattern obtained after calcination at 500 °C (Figure 4a) shows the formation of barium carbonate ($BaCO_3$) for the P_1 procedure, which is contrary to the second protocol where an amorphous phase appears. After calcination at 800 °C, a cubic perovskite phase of $BaTiO_3$ was identified by XRD (Figure 4b) for both protocols. However, for the P_1 procedure, the $BaCO_3$ phase is also present. Wang et al. also mentioned the formation of $BaTiO_3$ up to 800 °C with the acetic acid synthesis method[35] as well as the formation of $BaCO_3$ as an intermediate during the synthesis. The advantage of the P_2 procedure presented in this work is the avoidance of the formation of $BaCO_3$. This last procedure was used to create the coating.

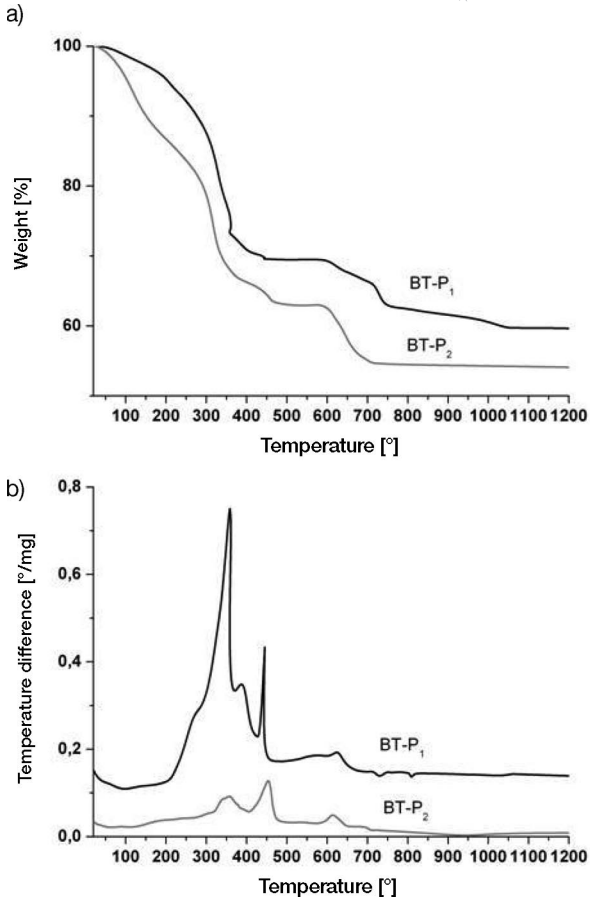

Figure 3. a) Thermogravimetric and b) differential thermal curves of $BaTiO_3$-PR1 and $BaTiO_3$-PR2.

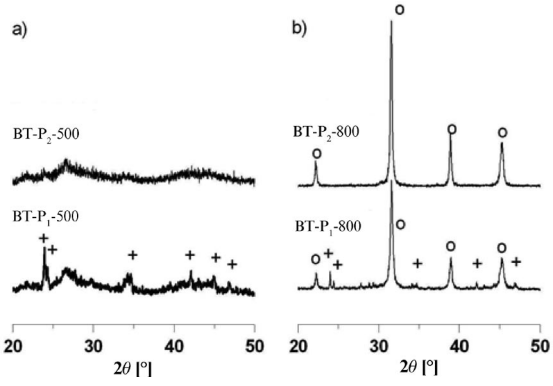

Figure 4. XRD patterns for the different protocols with an annealing temperature of a) 500 °C and b) 800 °C. (PDF files: o $BaTiO_3$ 79–2263 and + $BaCO_3$ 56–1471).

Shape-Formed Samples

LiTiNiO

For all spherical pellets, intermediate curing temperatures were tested before the final heating treatment at 500 °C, which must be performed to form the desired phase. The notations used for all the deposits are given in Table 4 in the Experimental Section. The amount of deposit is a

function of annealing temperature between each impregnation, as reported in Table 2. Successive impregnations with an intermediate thermal treatment at 250 °C (N^{o}_{2225}-s_a; see Experimental Section and footnote of Table 4 for notation) did not increase the amount of coating (around 10 wt.-%). On the contrary, at a temperature of 500 °C, the coating level reached 22 wt.-% after four impregnations (N^{o}_{5555}-s_a). In parallel, the amount of coating increased when calcination at 500 °C was first performed, followed by calcination at 250 °C after each impregnation and then finally one at 500 °C (N^{o}_{5225}-s_a). In fact, an intermediate phase could be formed during the first calcinations, which initiates the germination process and causes the following impregnations to be more efficient.

Table 2. Surface area and percentage deposit determined by gravimetric analyses or by elemental analyses using ICP (inductively coupled plasma) and the thickness for all spherical pellets synthesized.

Samples[a]	Deposit [%] gravimetric	ICP	Thickness of deposit [μm][b]	S_{BET} [$m^2 g^{-1}$]
Al_2O_3-500				180
Al_2O_3-800				166
N^{o}_{5}-s_a	10		3.2	–
N^{o}_{5555}-s_a	22		6.9	–
N^{o}_{2225}-s_a	11		3.5	–
N^{o}_{5225}-s_a	23		7.2	170
B^{o}_{8}-s_1	15		5.3	–
B^{o}_{888}-s_1	23		8.1	–
B^{o}_{228}-s_1	21		7.4	70
B^{o}_{8}-s_2N	4	4	1.4	–
B^{o}_{28}-s_2N	11	7	3.9	–
B^{o}_{228}-s_2N	12	10	4.2	70
B^{o}_{2228}-s_2N	12	12	4.2	–
B^{o}_{22228}-s_2N	10	13	3.5	–

[a] Material [drying method: classical oven (o) given as superscript; indication of the number and temperature of calcinations after each coating given as subscript; solution used given after hyphen]. [b] Calculated from the percentage deposit.

It can be noted that the surface area for the alumina balls N^{o}_{5225}-s_a is quite similar to that for the alumina balls sintered at 500 °C (Table 2), which implies that a partial deposit or diffusion in the ball has occurred. SEM micrographs (Figure 5a) reveal that deposition occurs only in a few areas and that the elements migrate into alumina balls up to a depth of 50 μm (Figure 5b). This diffusion explains the small amount of surface deposit. The thickness of a continuous deposit can be calculated from the percentage deposited according to Equation (2) where ρ, r_{ball}, $t_{deposit}$ and $m_{deposit}$ are the density of solid, the alumina ball radius, the deposit thickness and the deposit mass, respectively:

$$m_{deposit} = \frac{4\pi}{3}\cdot\rho_{deposit}\cdot[(r_{ball} - t_{deposit})^3 - r_{ball}^3] \quad (2)$$

In the case of the N^{o}_{5225}-s_a balls, a value of 23 wt.-% corresponded to a thickness of only 7 μm for the deposit (Table 2). Therefore, a depth of 50 μm implies a mixture of alumina and $Li_{0.10}Ti_{0.02}Ni_{0.88}O$, as identified by the XRD patterns (Figure 6) in which peaks attributable to NiO and alumina phases are present. Although the elements are diffused into the alumina balls, they do not seem to react with each other to form another phase. No additional studies were performed for this material because the aim of this work was to deposit a dielectric material on the surface of the alumina balls and not to study the impregnation volume of the dielectric materials. Nevertheless, the balls obtained could be interesting because an impregnation of NiO was effective up to 50 μm, which could allow an important number of active sites in a catalyst.

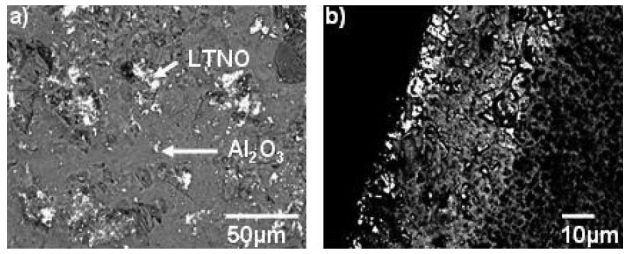

Figure 5. SEM micrographs of a) the surface and b) the ball cross section N^{o}_{5225}-s_a.

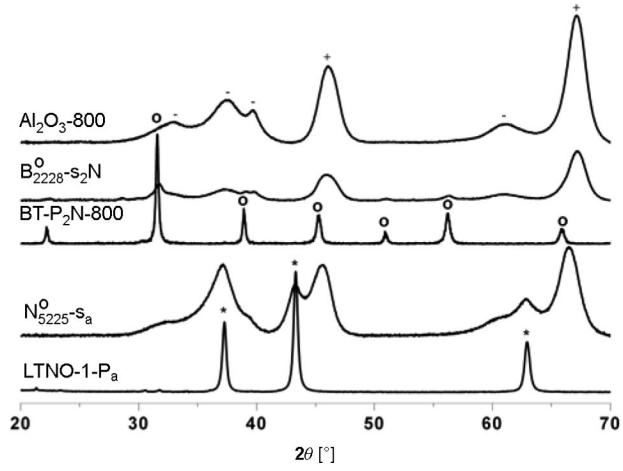

Figure 6. XRD patterns of B^{o}_{2228}-s_2N balls and N^{o}_{5225}-s_a balls in comparison with XRD patterns of alumina balls and powders synthesized by the approved protocol (PDF files: *: NiO 78–0429, o: $BaTiO_3$ 79–2263, +: γ-Al_2O_3 50–0741, –: δ-Al_2O_3 56–1186).

$BaTiO_3$

The deposition of $BaTiO_3$ over alumina balls was performed by the initial procedure described in the Experimental Section (notation of the materials is given in Table 4). Between two impregnations, annealing temperatures of 250 °C (B^{o}_{228}-s_1) and 800 °C (B^{o}_{888}-s_1) were selected. In both cases, the deposited quantities are similar (Table 2). It was possible to anneal at a temperature of only 250 °C between each impregnation. The variation in the amount deposited was interesting because from an initial deposit of 15 wt.-% (B^{o}_{8}-s_1), about 22 wt.-% was reached, which represents an efficient deposition method corresponding to calculated deposits of 4 μm (Table 2). The SEM micrographs (Figure 7a)

show that the deposit is not uniform since a local deposit of about 5 μm in depth is observed (Figure 7b), which is in accordance with the calculated deposit rate using Equation (2). In fact, the $BaTiO_3$ precursor adhered to the $BaTiO_3$ phase already deposited with a critical deposit thickness (Figure 7c). To enhance the quality of deposition, the coating protocol was modified, such as the drying method, the solution used to coat and to specifically treat the balls, which is presented in the next section.

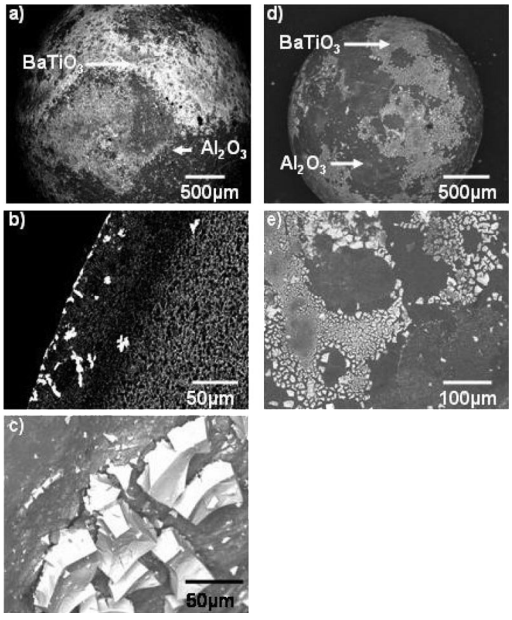

Figure 7. SEM micrographs of a) surface, b) section and c) surface zoom of the balls dried with a classical oven (B^{o}_{228}-s_1), and d) surface and e) surface zoom of balls dried with a microwave oven (B^{μ}_{8}-s_1).

Improvement of the Coating Process for $BaTiO_3$

Drying Method

Two drying methods were tested to improve the coating of the balls: a classical oven or a microwave oven drying method. The microwave oven was used to induce dielectric drying of the balls. The SEM micrographs of samples dried with a classical oven (B^{o}_{228}-s_1, Figure 7a) and with the microwave oven (B^{μ}_{8}-s_1, Figure 7d) show that the best results are obtained when the drying was performed in a classical oven. In fact, microwave treatment damaged the deposit because of excess energy, which resulted in fractured plates (Figure 7e). These plates indicate that many deposits were removed. For all future coating experiments, the use of a classical oven was chosen to perform the drying.

Composite Solution Use for the Coating of $BaTiO_3$

Another manner in which the quality of the coating could be enhanced is to improve the solution used. While preparing several composite solutions, the coating and drying steps were carried out in a rotary evaporator. The first solution consisted of the composite liquid system $BaTiO_3$ powder/glacial acetic acid. In order to achieve efficient adherence of the deposit, butvar (BTV) as binder, ethyl methacrylate (EMA) as dispersant medium and methyl ethyl ketone (MEK) as wetting agent were added to the solution.[36,37] BTV, a polyvinyl alcohol, is often used in the synthesis of dielectric materials since it allows an increasing in the green density.[38] MEK and EMA were used because of their chemical compatibilities with BTV.[39,40] The SEM micrographs (Figure 8a) of the balls obtained (B^{r}_{8}-p8) show that only a small surface of the balls was covered. Moreover, the deposit was only present in the pores of the alumina balls, where it created agglomerates (Figure 8b).

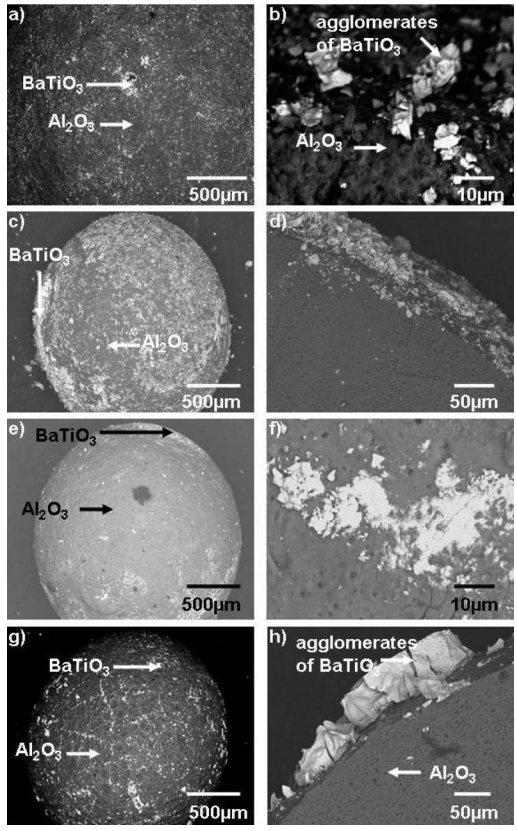

Figure 8. SEM micrographs of ball surface and section coating with different composite solutions: a) and b) powders annealed at 800 °C (B^{r}_{8}-p8), c) and d) powders annealed at 500 °C (B^{r}_{8}-p5), e) and f) powders annealed at 800 °C with sol (B^{r}_{8}-s_2p8), g) and h) powders annealed at 500 °C with sol (B^{r}_{8}-s_2p5).

The second composite solution contained a powder previously annealed at 500 °C instead of 800 °C to favour interactions between the balls and the pseudo calcinated powder. The same protocol and the same additives as used for the first solution have been used. We sought to obtain a reaction between alumina and the powders during the annealing process in order to create chemical absorption. The results were not efficient. SEM analyses shows that the deposit of $BaTiO_3$ was not continuous (Figure 8c). Furthermore, a friable deposit was obtained (Figure 8d), which showed physical adsorption.

Composite solutions created from a mixture of an initial sol used for synthesis and powders annealed either at 800 °C or at 500 °C were prepared with the same protocol and the same additives. The use of the powders gave the balls B_8^r-s_2p8 and B_8^r-s_2p5. The SEM micrographs again show the formation of a heterogeneous deposit (Figure 8e and g). In the case of the $BaTiO_3$ powder (B_8^r-s_2p8), the deposit was almost missing (Figure 8f), whereas it formed huge agglomerates of more than 50 μm size (Figure 8h) when powders annealed at 500 °C (B_8^r-s_2p5) were used. Therefore, the use of composite solutions did not enhance the quality of the coating. Indeed, the composite solution reacted more with powders present in the coating solution than with the alumina support. The best results were obtained with solely using the sol. This protocol was therefore continued, and an investigation on a step to fix the coating on the alumina balls was made.

Chemical Treatment of Wet Coating Balls

Initially, treatment of the alumina ball support was implemented. The surface of the support plays an important role in the feasibility of a homogeneous deposit. To favour the necessary interactions between the required material and the ball support, the sol solvent was used to wash the alumina balls. The balls were dipped in acetic acid and put in an ultrasound bath for 15 min. Alumina balls with or without a washing in acetic acid were analyzed by infrared spectroscopy (Figure 9). For alumina balls, only a peak at 1377 cm^{-1}, which is characteristic for γ-alumina in accordance with XRD analyses, was observed, since a minor amount of δ phase was present.

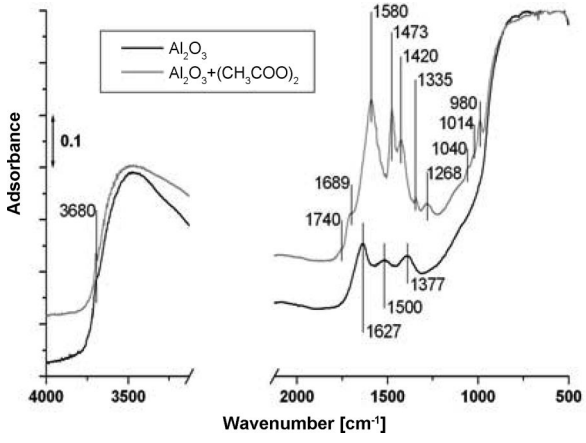

Figure 9. IR spectra of unwashed and washed (acetic acid/ultrasound bath) alumina balls.

The infrared spectrum of the alumina balls displays two peaks at 1500 cm^{-1} and 1627 cm^{-1}, which are attributed to the carbonate and water groups. The washing of the balls involved the formation of free OH species, with a peak at 3680 cm^{-1}, at the expense of carbonate species, as the surface was cleaned. Morterra et al.[41] explained this phenomenon as a change in the relationship between the acidic and the basic groups. Furthermore, some additional bands are present; three strong adsorption bands located at 1590, 1473 and 1420 cm^{-1} and three weak adsorption bands at 1335, 1040 and 1026 cm^{-1} are due to the presence of acetate species.[42] The acetate groups could reveal the formation of oxonium cations, which modify the superficial structure of alumina and cause a better adherence of the deposit.[43] The washing of alumina balls therefore permitted us to clean the surface and to create species such as free OH or oxonium cations, which could favour interactions with the sol.

The initial coating process was carried out, but the alumina balls were washed with acetic acid, and a new step was added between impregnation and drying of the balls (Scheme 1). Just after the impregnation step in the initiator sol, the balls were put into an aqueous ammonia solution (35%). This step was already implemented in some preliminary works on "oil-drop" shape forming.[18] In fact, the ammonia solution reacted with the acetic acid contained in the coating, which enables soft drying. To the first sol used for coating (s_1), MEK and BTV, but not the dispersant medium EMA, were added. The resulting balls (B_8^g-s_1N) did not reveal any deposit after annealing (Figure 10a). Another sol, containing all the three additives (s_2), was used for the impregnation step and deposits were obtained efficiently (Figure 10b). Indeed, because of its dispersant effect, EMA prevented the $BaTiO_3$ precursor from reacting too much with itself during ripening, which promotes strong interaction with the support. The state of the deposit was followed by gravimetric (Table 2) and SEM analyses (Figure 9b, c, d, e). The SEM micrographs indicate a fine dispersion of $BaTiO_3$ on the surface for the first four deposits (B_{28}^g-s_2N, B_{228}^g-s_2N, B_{2228}^g-s_2N) and disclose the appearance of cracks in the case of the fifth deposit (Figure 10e). Therefore, the number of deposits of $BaTiO_3$ carried out in accordance with Scheme 1 was limited to four. This limitation could be explained by the thickness of the deposit. A large value for the thickness resulted in more interactions with ultrasound during the following coating process, which led to the removal of the deposit. The best dispersion rate was therefore observed for the fourth coating (Figure 9d).

For these samples, elementary analyses using ICP have been performed (Table 2). A similar trend for the values obtained by ICP and by gravimetric analyses was found up to the third coating, even though the values are a little different. Important differences appeared with the fourth coating. Nevertheless, data obtained by gravimetric analyses for the first three deposits can be compared with the analytical data obtained for other coatings. An inconsistency appears when the third coating from the modified protocol (B_{228}^0-s_2N) is compared to the third coating from the initial process (B_{228}^0-s_1). A better dispersion is noticed for the former than for the latter, although the mass deposited increases more for the latter (21 wt.-%) than for the former (14 wt.-%).

Comparison between these two series of coated alumina balls can be completed by the measurement of the BET surface area. Alumina balls and $BaTiO_3$ powder have spe-

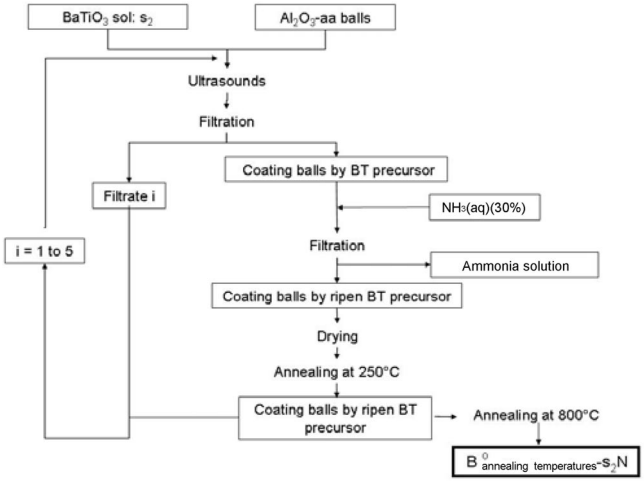

Scheme 1. Preparation of alumina balls coated with $BaTiO_3$ by the sol–gel process including an intermediary treatment with ammonia solution.

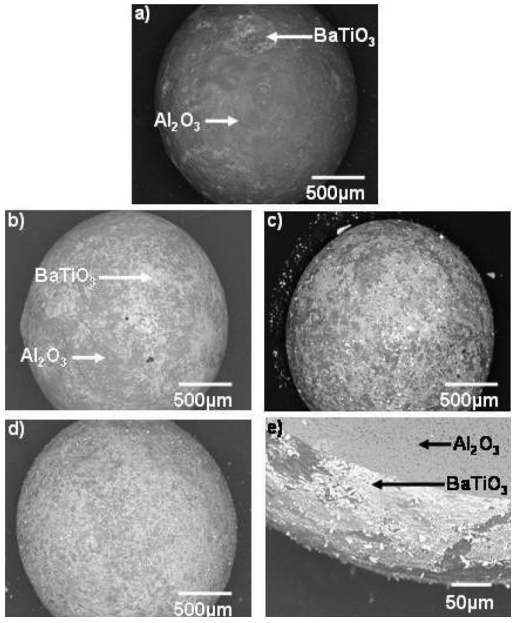

Figure 10. SEM micrographs of balls made by NH_3 treatment without EMA: a) one coating (B^0_8-s_1N), and with EMA: b) two coatings (B^0_{28}-s_2N), c) three coatings (B^0_{228}-s_2N balls surface), d) four coatings (B^0_{2228}-s_2N), and e) five coatings (B^0_{22228}-s_2N).

cific surface areas of 160 $m^2 g^{-1}$ (Table 2) and 10 $m^2 g^{-1}$ (Table 1), respectively. Therefore, the more the alumina support was covered by the deposit, the more the surface area decreased, down to a value of about 10 $m^2 g^{-1}$ for a continuous deposit. In addition, the balls B^0_{228}-s_1 and B^0_{228}-s_2N have the same BET surface area of 70 $m^2 g^{-1}$, although the quantity of $BaTiO_3$ deposited for the B^0_{228}-s_1 balls is greater than that for the B^0_{228}-s_2N balls. A similar surface area for a smaller quantity deposited thus implies a well-dispersed coating. Notably, the coating is not continuous because the BET surface area remains relatively high compared to that of the powders. An XRD analysis (Figure 6) of these balls also reveals a phase mixture of alumina and $BaTiO_3$. The same peaks as for the powder can be identified for the $BaTiO_3$ phase, and no peaks caused by a spinel could be identified.

In order to characterize the deposit more precisely, the cut of a B^0_{2228}-s_2N ball, made in agreement with the proposed procedure, was investigated with a Raman spectrometer equipped with microscope optics. A mapping from the surface to the inside of the ball was compared to the spectra of the synthesized $BaTiO_3$ powder and alumina (Figure 11). Under these analysis conditions, no peak appeared for alumina. The peak located at around 308 cm^{-1} is typical for the tetragonal $BaTiO_3$ phase and the three broad peaks at 255, 518 and 718 cm^{-1} could correspond to either the cubic or tetragonal $BaTiO_3$ phase,[23] which confirms the $BaTiO_3$ coating. Nevertheless, as explained before, Raman spectroscopy alone cannot be used to identify the phase, but the mapping performed by Raman spectroscopy allows an estimation of the thickness of the deposit. The mapping reveals the presence of the $BaTiO_3$ phase until a thickness of 5 µm, which is in accordance with the value calculated from the amount deposited (Table 2). Indeed, the deposit of the B^0_{2228}-s_2N balls was around 12 wt.-%, which corresponds to a calculated thickness of 4.2 µm for a continuous deposit.

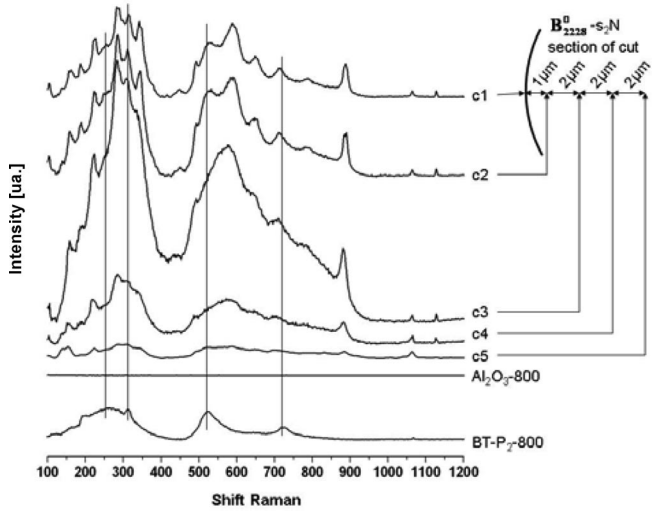

Figure 11. Raman spectra of $BaTiO_3$ powders, alumina balls and the cut of balls of B^0_{2228}-s_2N.

Several steps were thus necessary to obtain efficient deposition of $BaTiO_3$ over alumina balls from impregnation in a sol. In order to fix the deposit, a washing of the support in acetic acid was investigated. A binder was also used in this process, which implies the use of a wetting agent and, specifically, the use of a dispersion medium to avoid the formation of agglomerates. These additional agents should be removed from the support after the fixing process. Finally, a wetting of the coated balls in ammonia solution was performed to ensure soft drying before annealing.

In fact, compliance of every part of these experimental conditions is required to perform a spherical deposit of a $BaTiO_3$ perovskite similar to the synthesized powders. This protocol is effective, since it avoids the formation of Ba_2-

TiO_4 or TiO_2 phases, as mentioned by J. Zeng et al.[21] It can also be compared with that reported by Y. Keat et al.,[22] where a thin film with a relative permittivity lower than that of the corresponding pellets and with perovskite structure was obtained by the use of a stoichiometric excess. Furthermore, thin films of PBST (PbBaSnTi) and BZT (BaZnTi) compounds display efficient dielectric constants.[20,23] Consequently, the literature data suggest that the spherical deposit obtained should present competent reactivity in a plasma reactor since these materials should display efficient dielectric properties, as required. In addition, it is very difficult to compare our results with the results reported in the literature since all those deposits were made on wafers or on a planar surface and not on a spherical support. The use of a modified sol–gel method with additives has contributed to the feasibility and to the development of spherical deposits, which could be promising for plasma applications.

Conclusions

The syntheses of $BaTiO_3$ and $Li_xTi_yNi_{1-x-y}O$ materials by the sol–gel method, which are reported in this work, were successful. The use of several methods of characterization in this study, such as SEM, XRD, Raman spectroscopy and gravimetric analyses, showed the importance of each one in order to avoid false interpretations. In the case of nickel oxide doped with lithium and titanium, the deposit on alumina balls by coating in the sol involved an impregnation zone with a depth of more than 50 μm after four coatings. It is important to note that the first deposit had to be annealed at 500 °C to form an intermediate phase, which allowed the compound to adhere on the alumina. For the $BaTiO_3$ compound, the importance of the solvent was shown, and only the use of acetic acid gave a single cubic phase without carbonate. The coating on the alumina balls was not efficient with a simple coating in the sol. Moreover, neither drying methods nor mixed solutions enhanced the quality of the deposit. Nevertheless, a ripening of the coating in ammonia solution, together with a wetting of the support in acetic acid, allowed us to obtain a homogeneous deposit of $BaTiO_3$ of about 5 μm.

This study allowed us to obtain, for the first time, a spherical deposit of a dielectric compound by an adapted sol–gel method.

Experimental Section

Samples Preparation

The conditions for each synthesized powder sample are summarized in the Table 3.

Table 3. Notations for the powder compounds.

Sample notation	Compound	Solvent	$T_{annealing}$ / °C
LTNO-1-P_a	$Li_{0.100}Ti_{0.020}Ni_{0.880}O$	citric acid	
LTNO-1-P_a-500			500
LTNO-2-P_a	$Li_{0.222}Ti_{0.045}Ni_{0.733}O$	citric acid	
LTNO-2-P_a-500			500
LTNO-1-P_b	$Li_{0.100}Ti_{0.020}Ni_{0.880}O$	water + ammonia solution + ethanol	
LTNO-1-P_b-500			500
BT-P_1	$BaTiO_3$	water	
BT-P_1-500			500
BT-P_1-800			800
BT-P_2	$BaTiO_3$	acetic acid	
BT-P_2-500	$BaTiO_3$		500
BT-P_2-800			800

For the syntheses of LTNO materials, a solution of titanium(IV) diisopropoxide acetylacetonate (in 2-propanol 75%, Chempur), lithium nitrate (purity 99%, Aldrich) and nickel acetate (purity 99%, Aldrich) were used as precursors, and citric acid (purity 99%, Aldrich), distilled water, ethanol and ammonia solution (16.7 M; Carlo Erba) were used as solvents. In the first procedure P_a, titanium(IV) diisopropoxide acetylacetonate was added dropwise to a solution of lithium nitrate and nickel acetate dissolved in citric acid. The solution obtained was named s_a. Two proportions of doping agent were applied in this procedure: $Li_{0.10}Ti_{0.02}Ni_{0.88}O$ (LTNO-1) and $Li_{0.222}Ti_{0.045}Ni_{0.733}O$ (LTNO-2). The second procedure P_b was explained by Lin et al.[41] All precursors were added simultaneously in water. After dissolution, ammonia solution and ethanol were added successively.

In the case of the $BaTiO_3$ materials, the starting solutions were prepared from a solution of titanium(IV) diisopropoxide acetylacetonate (in 2-propanol 75%, Chempur) and barium acetate (purity 99%, Aldrich). Pure distilled water and glacial acetic acid (purity 98%, Aldrich) were used as solvents. Three experimental procedures were adapted by varying the addition order of the precursors and varying the solvent. After complete dissolution of barium acetate in water, the P_1 procedure consisted of a dropwise addition of the titanium solution, whereas acetic acid with a small amount of water [molar ratio $Ba(CH_3COOH)_2$/aa/H_2O = 1:10.6:5.19] was used as solvent in the P_2 procedure. In the P_3 protocol, all precursors were added simultaneously in acetic acid. The metal precursors for barium and titanium were chosen depending on their reactivity and solubility in common solvents. The ease of solubility of the barium precursor in glacial acetic acid involved the formation of the highly stable, stoichiometric precursor solution. Acetic acid acted as a donor ligand to titanium alkoxide and controlled hydrolysis and poly-condensation reactions.[43] Water was added to initiate the hydrolysis of the titanium precursor.[44]

For each preparation, an orange gel and a green gel for the $BaTiO_3$ and LTNO materials, respectively, were obtained after evaporation of the excess solvent. After drying in a ventilated oven overnight, the samples were annealed at 500 °C or 800 °C for 2 h, in static air on platinum crucibles with a heating rate of 5 °C min^{-1}.

Initial Process for the Coating of the Al_2O_3 Balls

Commercial alumina balls (Axens Gard, France) were used as coating supports. These balls were previously annealed at 800 °C and

Table 4. Notations and reaction conditions for the coated alumina balls.

Sample[a]	Coating Number	Annealing after each coating [°C]	Drying method	Precursor[b]/treatment	Support[c]
N^{o}_{5}-s_a	1	500	oven	s_a	Al_2O_3-5
N^{o}_{5555}-s_a	4	500, 500, 500, 500	oven	s_a	Al_2O_3-5
N^{o}_{2225}-s_a	4	250, 250, 250, 500	oven	s_a	Al_2O_3-5
N^{o}_{5225}-s_a	4	500, 250, 250, 500	oven	s_a	Al_2O_3-5
B^{o}_{8}-s_1	1	800	oven	s_1	Al_2O_3-8
B^{o}_{888}-s_1	3	800, 800, 800	oven	s_1	Al_2O_3-8
B^{o}_{228}-s_1	3	250, 250, 800	oven	s_1	Al_2O_3-8
B^{μ}_{-8}-s_1	3	–, -, 800	Microwave	s_1	Al_2O_3-8
B^{r}_{8}-p5	1	800	Rotavapor	p5	Al_2O_3-8
B^{r}_{8}-p8	1	800	Rotavapor	p8	Al_2O_3-8
B^{r}_{8}-s_2p5	1	800	Rotavapor	p5 + s_2	Al_2O_3-8
B^{r}_{8}-s_2p8	3	250, 250, 800	Rotavapor	p8 + s_2	Al_2O_3-8
B^{o}_{8}-s_1N	1	800	oven	s_1/NH_3	Al_2O_3-8-aa
B^{o}_{8}-s_2N	1	250, 800	oven	s_2/NH_3	Al_2O_3-8-aa
B^{o}_{28}-s_2N	2	250, 800	oven	s_2/NH_3	Al_2O_3-8-aa
B^{o}_{228}-s_2N	3	250, 250, 800	oven	s_2/NH_3	Al_2O_3-8-aa
B^{o}_{2228}-s_2N	4	250, 250, 250, 800	oven	s_2/NH_3	Al_2O_3-8-aa
B^{o}_{22228}-s_2N	5	250, 250, 250, 250, 800	oven	s_2/NH_3	Al_2O_3-8-aa

[a] Material [drying method: classical oven (o), microwave oven (μ) and rotary evaporator (r) given as superscript; indication of the number and temperature of calcinations after each coating given as subscript; solution used given after hyphen]. [b] s_a: sol of LTNO, s_1: sol of BT + MEK (7.81%) + BTV(15.62%), s_2: sol of BT + EMA (7.81%) + MEK (7.81%) + BTV (15.62%), p5: powders calcinated at 500 °C, p8: powders calcinated at 800 °C. [c] Al_2O_3-5: alumina balls calcinated at 500 °C, Al_2O_3-8: alumina balls calcinated at 800 °C and impregnated in acetic acid.

at 500 °C for 2 h in static air for the deposition of $BaTiO_3$ and $Li_{0.1}Ti_{0.02}Ni_{0.88}O$ (Table 4). The procedure consisted of dipping the balls into a sol and stirring with ultrasound with a frequency of 25 kHz in two steps of 15 min separated by a 15-min break. This was then filtered. The sol was put aside to perform other impregnations, whereas the coated balls were placed in an oven overnight at 120 °C for drying. After the thermal treatment, the balls wereagain placed in the sol and the procedure was repeated. After successive impregnations, the balls were finally annealed at 800 °C and at 500 °C for the $BaTiO_3$ and $Li_{0.1}Ti_{0.02}Ni_{0.88}O$ materials, respectively.

The sols obtained from the P_a and P_2 procedure were used to make balls with deposits of $Li_{0.1}Ti_{0.02}Ni_{0.88}O$ and $BaTiO_3$, respectively. To ensure an efficient coating, an amount of 8 wt.-% of methyl ethyl ketone (MEK) (≥99% GC, Aldrich) was introduced as wetting agent. A binder, Butvar B-98 (BTV) (Sigma), was also added in proportions of 2 wt.-% in 10 wt.-% ethanol solution. The sols obtained were named s_a and s_1 for $Li_{0.1}Ti_{0.02}Ni_{0.88}O$ and $BaTiO_3$, respectively. Different thermal treatments were applied between the impregnations (Table 4). For the $Li_{0.1}Ti_{0.02}Ni_{0.88}O$ material, the N^{o}_{5555}-s_a, balls were annealed at 500 °C after each impregnation, whereas the N^{o}_{2225}-s_a balls were annealed at 250 °C between two impregnations and at 500 °C after the last impregnation. In the case of N^{o}_{5225}-s_a balls, calcination was carried out at 500 °C after the first coating, at 250 °C after the second coating and at 500 °C after the last coating. For the $BaTiO_3$ compound, the balls were annealed either at 250 °C or at 800 °C between two impregnations. A curing at 800 °C was performed after the last coating.

Improvement of the Coating of the Al_2O_3 Balls by $BaTiO_3$

The initial process was modified to improve the coating of the alumina balls with $BaTiO_3$ material. Several modifications such as the precursor solution used for the coating, the treatment of the support, the method of drying and additional steps in the process were tested. The conditions for each sample are reported in the Table 4. For example, the B^{o}_{228}-s1 balls are alumina balls that were coated with sol s1, dried in an oven and annealed at 250 °C after the first and the second impregnation and at 800 °C after the third impregnation.

Achievement of the $BaTiO_3$ Precursor Solution: In each case, sample preparation was initiated with the preparation of the precursor of the $BaTiO_3$ compound solution. Afterwards, the above-mentioned additives were added to the precursor solution. The initial sol (s_1) contained MEK (8 wt.-%) and BTV (2 wt.-%). A secondary solution (s_2) was prepared with MEK (12 wt.-%), BTV (12 wt.-%, added as 9.00 wt.-% ethanol solution) and ethyl methacrylate (EMA, 4 wt.-%, 99% Aldrich), which acted as dispersant medium.

Four homogeneous solutions formed by a powder–liquid system were also used as precursor of $BaTiO_3$. A $BaTiO_3$ sol had previously been dried at 120 °C for 6 h and had been annealed at 500 °C or 800 °C for 2 h, which resulted in grey and white powders, respectively. These powders were mixed with glacial acetic acid (molar ratio $BaTiO_3$: acetic acid = 1:16.36) and with the additives EMA, MEK and BTV (the same proportions as in the case of s_2 were kept). These systems were called p5 and p8, respectively. The other nonhomogeneous systems used as $BaTiO_3$ precursor materials were based on mixtures between the sol s_2 and powders obtained previously by calcination at 500 °C or 800 °C. These systems were called s_2p5 and s_2p8, respectively. In all cases, the ratio between the mass of $BaTiO_3$ corresponding to the powder and to the sol s_2 was 1:3.

Treatment of Alumina Ball Supports: Commercial alumina balls were used as support for the $BaTiO_3$ deposit. The balls were initially annealed at 800 °C for 2 h in order to avoid a modification of the phase during the coating process. The balls were also wetted in glacial acetic acid (Al_2O_3-aa) for 15 min in an ultrasound bath. After filtration, the balls were again used for coating.

Ammonia Solution Treatment: To allow a quick adherence of the deposit to the support, an additional step was added between im-

pregnation and the drying of the balls. Balls coated with the $BaTiO_3$ precursor were dipped in 30% ammonia solution (mass ratio Al_2O_3/solution NH_3 1:1) and placed in an ultrasound bath. The balls were then recovered by filtration. A letter N was added at the end of the name of the samples obtained (e.g.: B^{o}_{28}-s_2N).

Drying and Thermal Treatment: Each impregnation step was followed by drying and heating treatments. The drying was performed either in an oven (o), a microwave oven (μ) or a rotary evaporator (r). The rotary evaporator was used when nonhomogeneous solutions were employed. The microwave oven was used with the sol s_1 by following the initial process.

All samples were annealed for 2 h at 250 °C between coatings, with the exception of the balls dried in the microwave oven. In this case, no annealing was performed after drying, and the balls were directly used for another coating. A final calcination was carried out for 2 h at 800 °C. The thermal treatment was included in the sample label. The heating steps were indicated by the index 2 or 8 for 250 °C and 800 °C, respectively (Table 4).

Samples Characterization

The products were characterized by powder X-ray diffraction (XRD) with a Bruker AXS D8advance powder θ-θ diffractometer using Cu-K_α radiation (λ = 0.15418 nm). The XRD data were collected at a scanning mode with a step of 0.02° and a scanning rate of 0.02 °s^{-1} in the 2θ range 10–90° for powders, while the scanning rate used for balls was 0.0018 °s^{-1}. LaB_6 was used as standard. An automatic PDF library search (Powder Diffraction Files from ICDD) and match was conducted, by using the standard SEARCH and DIFFRAC software (Bruker), for crystalline phase identification purposes. The morphology of the final products was determined by scanning electronic microscopy (SEM) with a JEOL 5600 LV scanning electron microanalyzer. A carbon sputtering was initially performed over the samples. The specific surface area of the samples was determined by the BET method from the nitrogen adsorption isotherms at –196 °C with an automated Micromeritics Tristar 3000 apparatus after drying for 90 min at 350 °C. Differential thermal analysis (DTA) and thermogravimetric analysis (TGA) were recorded in order to characterize the solids. DTA–TGA experiments were carried out in a Pt crucible between 25 and 1350 °C with a SDQ 600 TA Instrument. The samples were heated in a dry airflow at 5 °Cmin^{-1}. The Raman spectroscopic experiments were performed with a Horiba Jobin Yvon Confocal Raman Spectrometer equipped with a microscope optics function. The excited laser line used was 514.52 nm, and the exposition time was 30 s. The amount of deposit was acquired either by gravimetric analyses or by elementary analyses using ICP. Gravimetric analyses consisted of the finding of the carrying weight for a representative number of alumina balls before and after coating. The proportions of Ba and Ti were measured by elementary analyses using ICP for a few samples and the deposit quantity was deducted.

Acknowledgments

The Centre National de la Recherche Scientifique (CNRS) and the CEA of Grenoble financially supported this work. The authors thank E. Colnay, D. Mesnard and S. Arrii-Clacens for their technical support.

[1] A. Bogaerts, E. Neyts, R. Gijbels, J. Mullen, *Spectrochim. Acta Part B* **2002**, *57*, 609–658.
[2] G. Weiping, J. Zhanpeng, *CALPHAD Comput. Coupling Phase Diagrams Thermochem* **2002**, *26*, 403–418.
[3] R. J. Cava, *J. Mater. Chem.* **2001**, *11*, 54–62.
[4] S. R. Kulkarni, C. M. Kanamadi, B. K. Chougule, *Materials Research Bulletin 40* **2005**, 2064–2072.
[5] M. Adamczyk, Z. Ujma, L. Szymczak, I. Gruszka, *J. Eur. Ceram. Soc.* **2006**, *26*, 331–336.
[6] H. Jeon, S.-K. Lee, S.-W. Kim, D.-K. Choi, *Mater. Chem. Phys.* **2005**, *94*, 185–189.
[7] L. Wang, L. Liu, D. Xue, H. Kang, C. Liu, *J. Alloys Compd.* **2007**, *440*, 78–83.
[8] Q. Tang, M. Shen, L. Fang, *Solid State Commun.* **2005**, *135*, 707–710.
[9] Ph. Sciau, G. Calvarin, J. Ravez, *Solid State Commun.* **1999**, *113*, 77–82.
[10] J. Sigman, P. G. Clem, C. D. Nordquist, *Appl. Phys. Lett.* **2006**, *89*, 132909.
[11] F. D. Morrison, D. C. Sinclair, J. M. Skakle, A. R. West, *J. Am. Ceram. Soc.* **1998**, *81*, 1957–1960.
[12] J. Lee, K. Park, K. Hur, S. Yi, S. Koo, *J. Am. Ceram. Soc.* **2006**, *89*, 3299–3301.
[13] H. Takahashi, Y. Numamoto, J. Tani, S. Tsurekawa, *Japanese J. Appl. Phys.* **2006**, *45*, 7405–7408.
[14] C. J. Brinker, G. W. Scherer, *Sol–Gel Science: The Physics and Chemistry of Sol–Gel Processing*, Academic Press, New York, **1990** .
[15] J. Wu, C.-W. Nan, Y. Lin, Y. Deng, *Phys. Rev. Lett.* **2002**, *89*, 217601.
[16] Z.-M. Dang, C.-W. Nan, *Ceramics International 31* **2005**, 349–351.
[17] V. Trovcova, I. Furar, F. Hanic, *J. Phys. Chem. Solids* **2007**, *68*, 1135–1139.
[18] B. Fournaud, B. Rossignol, S. Tatibouët, S. Thollon, *J. Mater. Technol. Process.*, in press.
[19] L. Guofeng, W. Zhiqiang, W. Ninghui, *J. Mater. Sci.* **2007**, *42*, 8242–8247.
[20] C. Kai-Huang, C. Ying-Chung, Y. Cheng-Fu, C. Ting-Chang, *J. Phys. Chem. Solids* **2007**, *68*, 4197–4201.
[21] J. Zeng, H. Wang, M. Wang, S. Shang, Z. Wang, C. Lin, *Thin Solid Films* **1998**, 322,104–107.
[22] Y. Keat, S. Sreekantan, S. D. Hutagalung, Z. A. Ahmad, *Mater. Lett.* **2007**, *61*, 4536–4539.
[23] S. Xiaohua, H. Huiming, W. Shengxiang, L. Meiya, Z. Xingzhong, *Thin Solid Films* **2008**, *516*, 1308–1312.
[24] C. J. Xiao, Z. H. Chi, W. W. Zhang, F. Y. Li, S. M. Feng, C. Q. Jin, X. H. Wang, X. Y. Deng, L. T. Li, *J. Phys. Chem. Solids* **2007**, *68*, 311–314.
[25] G. Busca, V. Buscaglia, M. Leoni, P. Nanni, *Chem. Mater.* **1994**, *6*, 955–961.
[26] H. Ikawa, T. Nakai, S. Higuchi, K. Saitoh, M. Takemoto, *Trans. Mater. Res. Soc. Jpn.* **2006**, *31*, 101–104.
[27] C. Woo-Seok, *J. Phys. Chem. Solids* **1998**, *59*, 659–666.
[28] K. Suzuki, K. Kijima, *J. Alloys Compd.* **2006**, *419*, 234–242.
[29] C. Pithan, Y. Shiratori, R. Waser, *J. Am. Ceram. Soc.* **2006**, *89*, 2908–2916.
[30] J. C. De Jesus, I. Gonzalez, A. Quevedo, T. Puerta, *J. Mol. Catal. A* **2005**, *228*, 283–291.
[31] S. Myoung Youp, L. Ryong, K. IkHyun, *Solid State Ionics* **2003**, *156*, 319–328.
[32] I. Oja Açik, J. Madarász, M. Krunks, K. Tonsuaadu, D. Janke, G. Pokol, L. Niinistö, *J. Therm. Anal. Calorim.* **2007**, *88*, 557–563.
[33] S. Maensiri, P. Thongbai, T. Yamwong, *Acta Materialia* **2007**, *55*, 2851–2861.
[34] *Handbook of Chemistry and Physics* 50th ed., The Chemical Rubber Company, Cleveland, **1970**, F152.
[35] L. Wang, L. Liu, D. Xue, H. Kang, C. Liu, *J. Alloys Compd.* **2007**, *440*, 78–83.
[36] Y.-S. Cho, J.-G. Yeo, Y.-G. Jung, S.-C. Choi, J. Kim, U. Paik, *Mater. Sci. Eng.* **2003**, *A362*, 174–180.
[37] J.-H. Hwang, B. I. Lee, D.-H. Kim, S.-K. Wi, *Colloids Surf. A: Physicochem. Eng. Aspects* **2006**, *289*, 60–64.

[38] D.-H. Yoon, B. I. Lee, *J. Eur. Ceram. Soc.* **2004**, *24*, 739–752.
[39] C. Morterra, G. Magnacca, *Catal. Today* **1996**, *27*, 497–532.
[40] M. A. Hasan, M. I. Zaki, L. Pasupulety, *Appl. Catal A: General* **2003**, *243*, 81–92.
[41] Y. Lin, L. Jiang, R. Zhao, C. W. Nan, *Phys. Rev. B* **2005**, *72*, 014103.
[42] M. Bartók, K. Balázsik, G. Szöllösi, T. Bartók, *Catal. Commun.* **2001**, *2*, 269–272.
[43] A. Kumar, S. Chauhan, V. Gupta, K. Sreenivas, *Mater. Sci. Eng. B* **2006**, *130*, 81–88.
[44] X. Xing, J. Deng, J. Chen, G. Liu, *J. Alloys Compd.* **2004**, *384*, 312–317.

Received: May 28, 2008
Published Online: October 21, 2008

